# Spectral Decomposition of Ultrawideband Terahertz Imagery*

E.N. Grossman[1], C. R. Dietlein[1,2], J. Chisum[1,2], and A. Luukanen[3]
J.E. Bjarnason[4], and E.R. Brown[4]
[1] Optoelectronics Division, National Institute of Standards and Technology, Boulder, CO
[2] Electrical and Computer Engineering Dept., Univ. of Colorado, Boulder, CO
[3] Millimetre-wave Laboratory of Finland, Tietotie 3, Espoo, Finland
[4] ECE Department, Univ. of California, Santa Barbara, CA

## ABSTRACT

We investigate the spectral response of a THz imaging system based on ultrawideband cryogenic microbolometers. The bandwidth if this system, nominally 0.2 – 1.8 THz, is broad enough to span large variations (>10 dB) in clothing transmittance and diffraction-limited spatial resolution (factor of x8), factors that are presumably partly responsible for the unusually high quality of the images taken with it. The chief tools we have used for this are a simple THz monochromator based on a specially designed frequency selective surface, and a specially designed blackbody source that provides an accurately known power spectral density over the full bandwidth of the imager. Two completely independent measurements of the microbolometer's spectral response, in the first case using a filtered blackbody and in the second using an ultrabroadband, THz photomixer, referred to a Golay cell, agree within 5%. Evidence of frequency-dependent scattering from ordinary clothing material, distinct from simple linear attenuation, is presented from an idealized laboratory experiment. However, the scattering is relatively weak, and unlikely to have a significant effect in practical THz imaging scenarios, particularly with ultrawide bandwidths.
**Keywords:** Bolometer, concealed weapons, imaging, millimeter-wave, terahertz, ultrabroadband

## 1. INTRODUCTION

As described elsewhere, we are currently developing a terahertz camera based on a large, mechanically scanned linear array of antenna-coupled, superconducting microbolometers[1, 2]. Early imagery taken with a single-pixel version of this camera (Fig. 1) shows a remarkably high capability for detecting and identifying threat items concealed beneath clothing. However, despite ongoing analysis being done on this imagery[3], it is still an open question as to what accounts for the (subjective) high quality of these images. Clearly a combination of good spatial resolution, high sensitivity (i.e. low NETD), and adequate clothing transmittance[4] is essential, but the relative importance of these factors is unclear. Moreover, these factors have opposite dependences on frequency, lower frequencies providing better penetration, but higher frequencies offering better spatial resolution. Therefore, it is not yet possible to identify the optimum frequency band for THz personnel screening, despite the question's obvious practical importance. Spectral decomposition of this type of imagery is needed in order to resolve that.

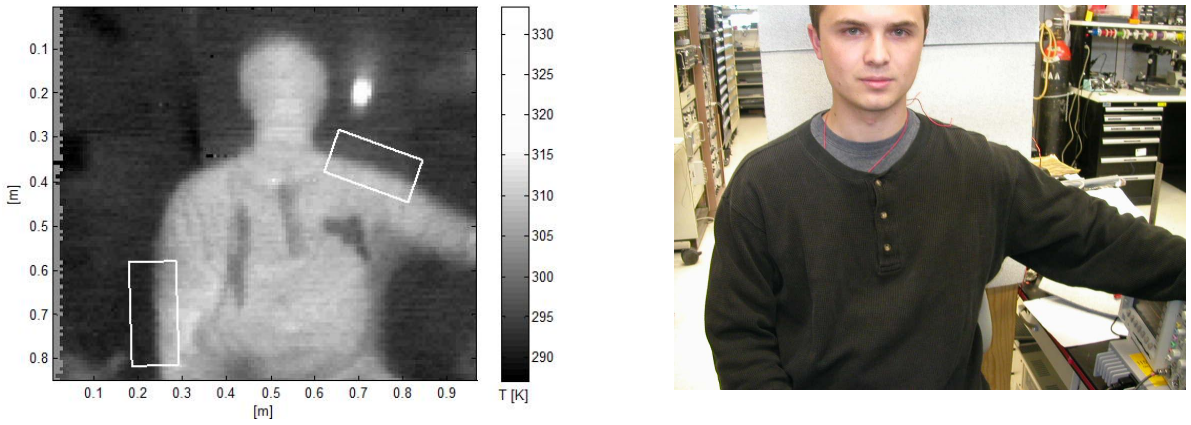


**Fig. 1. (left) Ultrawideband image obtained with mechanically scanned 0.1 – 1.2 THz microbolometer system. (right) corresponding visible image of same scene.**

* Contribution of the U.S. Government. Not subject to copyright.

Passive Millimeter-Wave Imaging Technology X, edited by Roger Appleby, David A. Wikner,
Proc. of SPIE Vol. 6548, 654807, (2007) · 0277-786X/07/$18 · doi: 10.1117/12.719632

## 2. SPECTRAL RESPONSE

The first step in addressing these questions is to understand of the spectral response of individual components of the system. The key elements are (a) the THz "circular variable filter" we have developed, which we use as a monochromator, (b) the microbolometer element, which is coupled through a hyperhemispherical substrate lens and spiral antenna, (c) the optical train, and (d) clothing.

### A. Circular Variable Filter

It is well known that an array of sub-wavelength, crossed slots in an electrically thin, conducting groundplane will act as a bandpass filter in transmission. This is a special case of a frequency-selective surface (FSS), which is widely used in the microwave band for radomes and other conformable electromagnetic structures[5]. This is a natural method for implementing a monochromator in the THz band, where interference filters would require prohibitively thick dielectric layers. Such filters based on FSS's have been demonstrated to frequencies above 2 THz with low insertion loss[6, 7] and are even available commercially. The monochromator used in the present work extends this idea to a continuously tunable filter by scaling the slot length, width, and period continuously around the circumference of a circle. The filter can then be rotated about the center of this circle to provide a spectral passband whose center frequency oscillates linearly in time between two limits. The design method is described in detail elsewhere[8]; the main complication is the finite electrical thickness of the substrate (25 μm, kapton). Because the substrate thickness does not vary with angle, but does affect the resonant frequency, the slot dimensions do not scale linearly with angle, as would be expected from simple self-similarity.

2 prototypes have been built, with octave bandwidths covering 220-440 and 110-220 GHz respectively. The CVF is characterized, for normally incident beams, by its transmittance as a function of frequency and angle. Angular scans were made on the lower frequency unit at 11 fixed frequencies from 110 to 220 GHz, and the transfer function inverted, to yield the spectral transmittance shown in Fig. 2b, for the fixed angular position corresponding (in this case) to 143 GHz center frequency. The spectral shape can be very roughly approximated by a Lorentzian and the center frequency and bandwidth extracted for the equivalent rectangular bandpass filter.

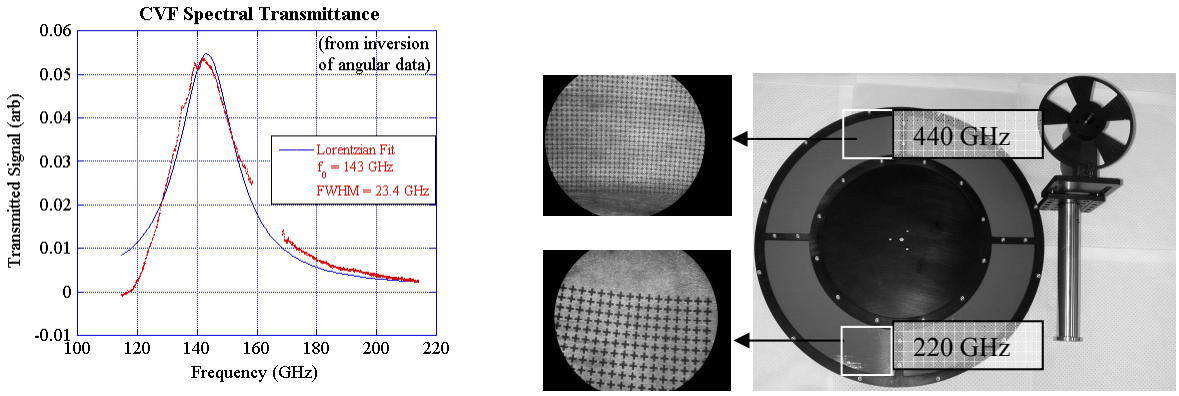


**Fig. 2. THz Circular Variable Filter. (left) Spectral transmittance at a fixed angle, obtained by inversion of transfer function measured on 110-220 GHz CVF, (right) photograph of assembled 220-440 GHz CVF.**

### B. Antenna-coupled Microbolometer

As described in ref. 1, the microbolometer is coupled to the incident field through a planar, equiangular spiral antenna and a Si hyperhemispherical substrate lens. The design bandwidth for the spiral, limited by the inner and outer radii at which the antenna's shape deviates from an equiangular spiral, covers 200 – 1800 GHz. (Note that this differs slightly from the 100 – 1200 GHz band covered by the original spirals used to obtain Fig. 1.) The antenna pattern has been measured at frequencies *f* of 95, 238, and 650 GHz[9]. The 3 dB full width is well approximated

in both linear polarizations and both angular planes by $\mathrm{FWHM} = \dfrac{4.50\ \mathrm{THz} - \mathrm{degrees}}{f}$ at 238 and 650 GHz. As discussed in ref. 9, the pattern at 95 GHz, (which is below the design bandwidth) is somewhat narrower and less regular than suggested by the above formula due to a contribution from a dipole-like component. Equating this measured beamwidth with that expected from a diffraction-limited, plane-wave illuminated aperture, ie. $\mathrm{FWHM} = 1.03\dfrac{\lambda}{D}$, where $\lambda$ is the wavelength and D the aperture diameter, yields an effective aperture diameter D = 3.9 mm, in nearly perfect agreement with the actual lens diameter of 4 mm. The broadband behavior of the lens-coupled spiral is thus well-described by a diffraction-limited, plane-wave illuminated aperture, in agreement with the early investigations of this "synthesized ellipse" configuration by Buettgenbach[10] and Filipovic[11].

### C. Optics

Besides the spiral antenna bandwidth, there is another significant difference between the system configuration when Fig. 1 was taken and the present. Specifically, the extension length of the substrate lens was originally d=0.58mm = 0.99R/n (where R is the lens' radius of curvature and n its refractive index); it is now d=0.83mm=1.41R/n. The original extension length corresponds to the lens' aplanatic point; the present length is very close to the "synthesized elliptical" point described in refs 10 and 11. Although there is relatively little difference between these configurations when used in a narrowband or moderate (sub-octave) bandwidth system, there could be a substantial difference in an ultrawideband system. Specifically, at the aplanatic point, the intrinsic angular pattern of the antenna, which due to the spiral's self-similar nature is frequency-independent, is simply narrowed by a factor of n in each direction. Thus, the resulting far-field angular pattern outside the substrate lens is also frequency independent. Therefore the aperture illumination is frequency independent, while the effective area of the antenna scales as $\lambda^2$. Since the focal plane is at an image of the target plane, the spatial resolution at the target likewise scales as $\lambda^2$. On the other hand, at the synthesized elliptical point, the far-field angular pattern outside the lens approximates an Airy pattern from of a plane-wave illuminated aperture of the same diameter as the lens. The angular pattern (FWHM) therefore scales with as $\lambda^2$. This is what the 238 and 650 GHz pattern measurements on the present configuration have confirmed. In this case, the aperture illumination also scales as $\lambda^2$. The outer regions of the primary optic are not illuminated at higher frequencies. The spatial resolution at the target is now frequency-independent, being simply the substrate lens diameter times the magnification of the optics.

The contrast between these two substrate lens configurations is completely analogous to that between scalar feedhorns and standard-gain pyramidal feedhorns. Scalar feedhorns have an effective area which is frequency-independent; their gain scales as $\lambda^{-2}$. Pyramidal feedhorns on the other hand, being self-similar, have a gain which is frequency-independent and an effective area that scales as $\lambda^2$. In the case of feedhorns, the consequences of this difference are ordinarily not dramatic, since the fractional bandwidth of systems based upon them is limited to a waveguide band ($f_{max}/f_{min} < 1.5$). In the case of the substrate lens-coupled spirals however, the system is designed to be ultrawideband, and the difference could be critical in determining the quality of the resulting imagery.

### D. Clothing

The fact that transmittance of typical clothing materials rolls off with frequency in the THz band is now well established (ref 4). This leads to the natural interpretation of Fig. 1 and similar images as superpositions of low frequency images with poor spatial resolution and deep penetration, and high frequency images with good spatial resolution and shallow penetration. However the question remains open whether the presence of clothing has any effects on THz imagery *besides* simple linear (Beer's Law) attenuation at high frequencies? All previously reported clothing transmittance measurements simply refer to power transmitted in the same spatial beam with and without the presence of clothing – they are thus not sensitive to scattering in particular. If significant, the THz scattering of clothing could introduce quite complex frequency dependence into THz images, given that most clothing is a periodic (woven) material with a period comparable to the wavelengths involved [14].

A simple scattering measurement, such as that shown in Fig. 3, is enough to show that this is an observable effect. Peaks in the scattered distribution are clearly observed at the angles predicted for first-order ($n = \pm 1$) grating lobes by the grating equation, $\sin\theta_i + \sin\theta_s = \dfrac{n\lambda}{P}$, where $P$ is the grating period, and $\theta_i$ and $\theta_s$ the incident and scattered

angles from normal. However, the question of whether such scattering will affect *typical* THz images *significantly* is quite different from whether it is observable. Firstly, the scattering displayed in Fig. 3 is not a dominant effect. Simply integrating the distribution shown in Fig. 3, we find the central "straight-through" peak displays a transmittance of 49.8% and 44.0% at normal and 5° incidence angles, respectively (statistical uncertainties are approximately $\pm$ 0.3% in both these figures). Of the 50.2% that is not transmitted in the normal incidence case, approximately 27% (i.e. 13.7% of the incident power) is scattered into the two first-order grating lobes combined. The remaining power is presumably absorbed, since there is no evidence in Fig. 3, or other scans over larger angular ranges, of additional scattering peaks. The two grating lobes do not show equal integrated powers, which we attribute to residual stray light in the test setup, at the ~1% level.

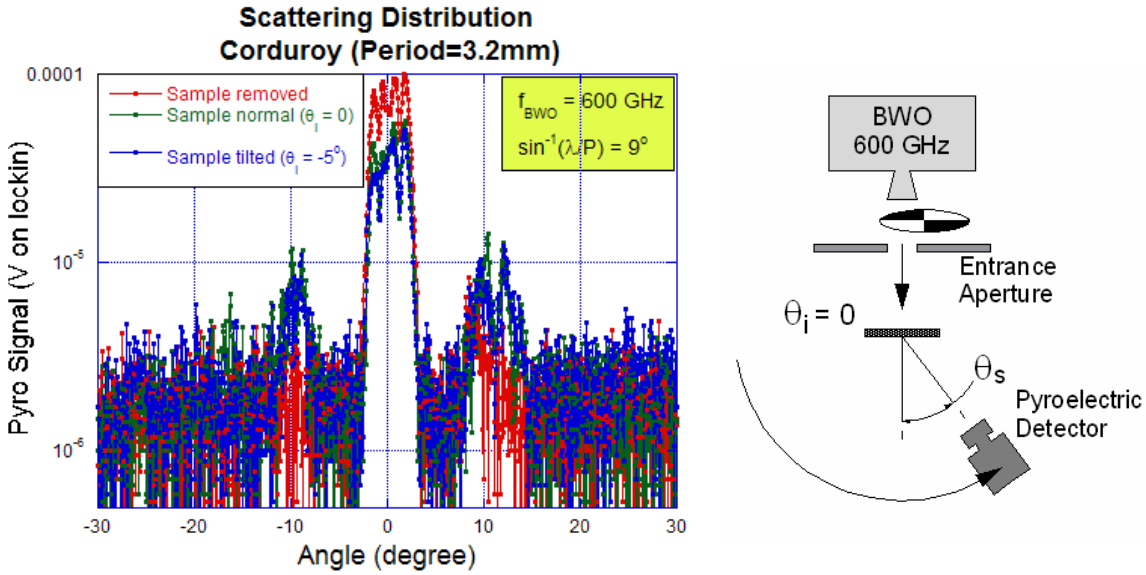


**Fig. 3 Angular scattering distribution from a sample of ordinary "8-wale" (ie. 8 lines per inch) corduroy at 600 GHz. The ripples visible in the transmitted peak are due standing waves between the entrance aperture and detector mount of the test setup.**

In an ordinary personnel screening geometry, the effect of the above would be that ~14% of the signal from a concealed object would appear to come from a position that is displaced from its true position by $d \tan \theta_S$ where d is the distance between the concealed object and the scattering screen (clothing). The displacement of this apparent "ghost object" is relatively small however (since $d$ is small), and not necessarily greater than the diffraction-limited spatial resolution of the imaging system. Moreover, in a passive imaging scenario, the scattering would be integrated over frequency; therefore, there would not be any discernable "ghost objects", simply small tails to the distribution of light emitted from the edges on an object, analogous to the penumbra of shadows, which might or might not broaden the edge beyond the limit set by diffraction.

It should be noted moreover, that the conditions of the measurement shown in Fig. 3 were specifically chosen to provide a larger scattering effect than would be typical. Most importantly, the ratio $\lambda/P$ was chosen to be at the low end of realistic values, since the strength of scattering peaks generally falls off rapidly as the scattering angle $\theta_S = \sin^{-1}\left(\frac{n\lambda}{P}\right)$ increases. In general, most of the useful THz response probably arises from longer wavelengths, and most clothing probably only displays periodicity on shorter length scales, than that used in the measurement of Fig. 3. Since the effect was only marginally significant even in that case, it seems quite unlikely that scattering effects would significantly degrade the effectiveness of THz imagery for concealed object detection in more typical cases.

## 3. SPECTRAL MEASUREMENTS

The first step in spectrally decomposing THz imagery is to thoroughly characterize the end-to-end spectral response of the imaging system. Though seemingly straightforward, this is in reality problematic, because there are very few scenes or sources in the THz band which are flat enough with frequency (or whose frequency dependence is well enough known) that they can be used as a *reference* for the spectral response of an unknown system. Therefore, we have simply performed two completely independent measurements, in separate labs, with completely different methodologies, and examined how well the results (for relative system response in different spectral bands) agree.

The first experiment was done by J. Bjarnason and E. Brown in the latter's THz spectroscopy laboratory at UC Santa Barbara. The ultrawideband THz photomixer[12] has a strongly frequency dependent output power, but that has been removed from the result shown in Fig.4 by normalizing the photomixer output to the response of a diamond-windowed Golay cell. The latter therefore forms the reference for the spectral response in this experiment.

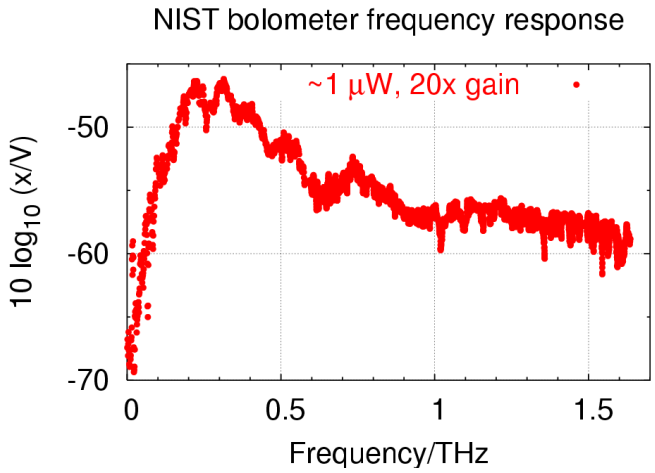


**Fig. 4. Spectral response of lens-coupled antenna with an uncooled Nb microbolometer at its feed, measured using the UCSB photomixer as a secondary transfer standard, to refer the microbolometer response to that of the Golay cell reference detector.**

The second experiment was done by using as a reference a specially developed THz source, which we call the Aqueous Blackbody Calibration (ABC) source, that is described at length elsewhere in these proceedings[13] . It is essentially a bath of hot, circulated water held in a specially shaped container of expanded polystyrene (EPS). The container's shape is designed to form an "optical trap" that ensures an extremely low reflectance (i.e. high emissivity) in the 100 – 1000 GHz range, despite the fairly high reflectance of a single water-EPS interface. A cryogenic microbolometer, with identical substrate lens and spiral antenna coupling as used in the UCSB experiment, was then used to form scanned images of the ABC source's entrance aperture, either directly, and therefore including the full cryogenic system bandwidth, or through specific locations on the THz CVF, thus including only the known spectral bandpass of the CVF. The beam from the ABC source was mechanically chopped with an ambient temperature absorber ( $T_{ABC} - T_{ambient} = 40K$ ) and the microbolometer signal synchronously detected. The resulting images are shown in Fig. 5. The trapezoidal shape of the hot region is due to perspective; at the relatively short range (~0.8 m) of the ABC source from the scanning mirror, this distortion is quite noticeable. The hot region appears considerably larger than the nominal entrance aperture, whose outline is superposed on each of the images. Within these adjacent regions, the radiometric temperature is close to the water temperature ( $T_{water} = 60^{o}$ C in all the images shown), but not accurately so -- a close examination of the image shows small (but significant compared to the noise) reductions in signal outside the entrance aperture. In any case, each of the filtered images was integrated over the area of the entrance aperture, and the resulting signals normalized to the integrated signal from the unfiltered system.

The resulting figures are summarized in Table 1. The effective bandwidths of the two spectral channels examined, 230 and 430 GHz (which correspond to the minimum and maximum available on the higher frequency CVF), are those of the equivalent rectangular bandpass to the fitted Lorentzians. Specifically, the CVF transmittance was

fitted to $T(f) = \dfrac{\gamma^2}{(f-f_0)^2+\gamma^2}$ and the effective bandwidth computed from $B = \int_0^\infty T(f)df = \gamma\left(\dfrac{\pi}{2} + \tan^{-1}\left(\dfrac{f_0}{\gamma}\right)\right)$.
This is given in the first row of table 1 and is equal to the ratio of power densities (W/cm$^2$) in the two spectral channels.

Integrating across the entrance aperture of the ABC source, the ratio of intensities from the filtered ABC images, $\dfrac{I_{430}}{I_{230}} = 1.12$ is much less than the ratio of bandwidths; this fact is highly significant compared to the uncertainty. Since the ratio of incident powers is simply the ratio of bandwidths, this difference simply reflects a lower system response at 430 GHz than 230 GHz. Indeed, the same ratio of system response at 430 GHz to 230 GHz can be extracted from the photomixer data simply by integrating the spectral data over the equivalent bandwidths. The result is $\dfrac{I_{430}}{I_{230}} = 1.07$. The level of agreement between these two measurements, within 5 % (0.2 dB) of one another, is quite remarkable given the total independence of the two experiments, and was not expected. The power level coupled to the detector (P=kTB) is in the 10's of pW range for the filtered blackbody measurement. We believe this level of radiometric accuracy represents the current state of the art for traceable power measurements in the THz band. It is also indicative of the minimum detectable strength of (broadband) spectral features that we expect to see in multispectral imagery obtained with the CVF and cryogenic microbolometer.

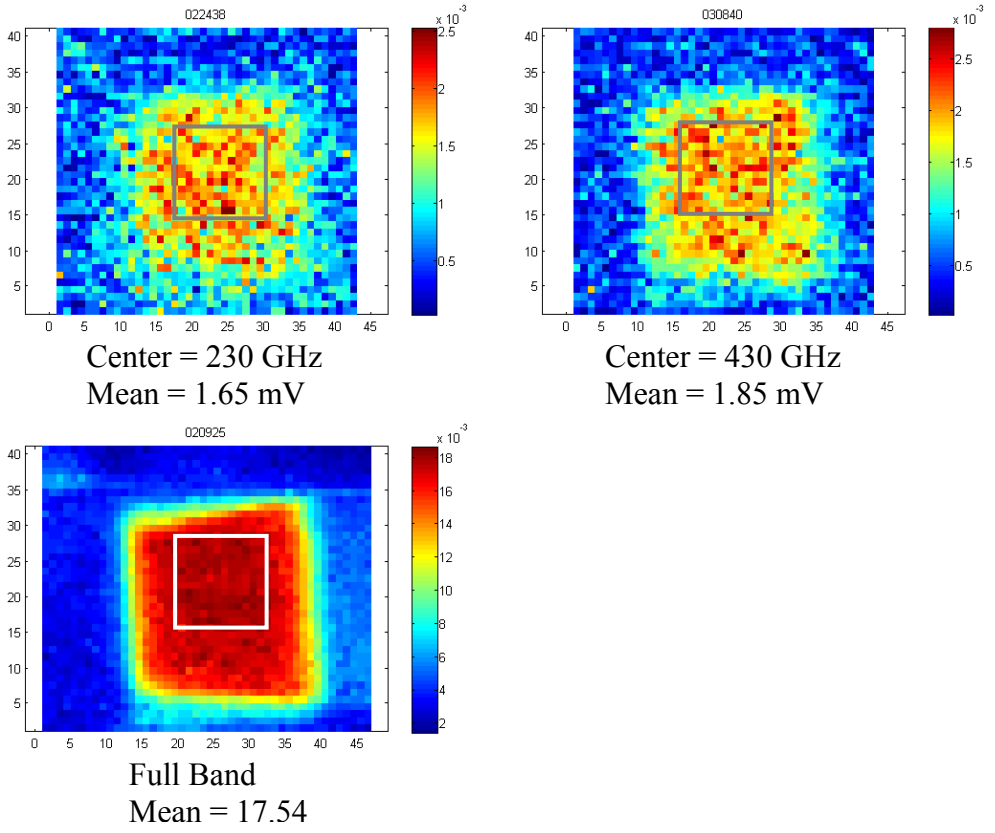


**Fig. 5. Images of the entrance aperture of the ABC source, taken within two representative passbands defined by the THz CVF, and over the full (unfiltered) bandpass of the cryogenic imager.**

The ratio of filtered responses to full (i.e. unfiltered) responses is given in the last two columns of table 1. In these cases, there is a slightly larger discrepancy between measurements from the photomixer experiment and the ABC source (16% and 20% respectively for the 230 and 430 GHz channels). However, this is in fact expected. It is

known, from FTIR measurements of the EPS material transmittance and analysis of its effect on radiometric accuracy (Dietlein ABC reference and to be published), that the brightness of the ABC source falls noticeably above 1 THz. This is not yet accurately characterized, but the brightness contrast against a room-temperature chopper is likely to fall from 40 C to ~30 C by 1.2 THz. Direct integration of the photomixer response indicates that a full 25% of the system response comes from frequencies > 1 THz. Thus the full, unfiltered system response is likely to be underestimated in the ABC source measurements, by on the order of 10 %.

| | Ratio: 430GHz/230 GHz | 230 GHz | 430 GHz |
|---|---|---|---|
| **Bandwidth (GHz)** | **1.86** | **58** | **108** |
| | | | |
| **Spectral response of system** | | $I_{230} / I_{full}$ | $I_{430} / I_{full}$ |
| **UCSB Photomixer** | **1.07** | **0.081** | **0.087** |
| **ABC Source and CVF Filter** | **1.12** | **0.094** | **0.105** |

**Table 1. Fraction of total system response contained within CVF Bands**

## 4. CONCLUSIONS

We have described a number of tools developed and measurements made in order to accurately decompose the spectral structure of images obtained with a lens/antenna-coupled, cryogenic microbolometer. The THz CVF forms a basic monochromator and the ABC source a spectrally flat reference; together they enable absolutely calibrated, ultrawideband, multispectral imaging at the pW power levels appropriate for passive indoor concealed object detection. Real ultrawideband images of personnel consist of superpositions of low frequency images with good clothing penetration but poor spatial resolution and high frequency images with shallower penetration but better spatial resolution. Scattering effects of clothing, distinct from simple linear attenuation, have been observed in an idealized laboratory situation. However, we have argued that in realistic imaging scenarios these are likely to be too small to significantly affect the effectiveness of THz imagers. A comparison between the spectral response of the system obtained from a photomixer-based measurement at UCSB and a filtered blackbody measurement at NIST indicates agreement at the 5% level.

## 5. ACKNOWLEDGEMENTS

This work at NIST is supported by the DHS Science and Technology Directorate. Development of the ABC source was stimulated by the needs of, and largely supported by, the DARPA MIATA program.

## 6. REFERENCES

[1] A. Luukanen, Erich N. Grossman, Aaron J. Miller, Panu Helist¨o, Jari S. Penttil¨a, Hannu Sipola, and Heikki Sepp¨a, "An Ultra-Low Noise Superconducting Antenna-Coupled Microbolometer With a Room-temperature Read-out," *IEEE Microwave and Wireless Components Letters* vol. 16, pp. 464-466, 2006.

[2] A. Luukanen, Panu Helistö, Jari S. Penttilä, Heikki Seppä, Hannu Sipola, Charles R. Dietlein, and Erich N. Grossman, "An array of superconducting antenna-coupled microbolometers for passive video-rate THz imaging," *Proc. 4th ESA Workshop on Millimetre-wave Technology and Applications*, pp. 417-422, 2006.

[3] M. Ramirez-Velez, Ditelein, C., Grossman, E., and Popovic, Z., "Unsupervised Segmentation and Classification of THz Images," *Proc. SPIE*, vol. this issue, 2007.

[4] J. E. Bjarnason, Chan, T. L. J. , Lee, A. W. M.,Celis, M. A., Brown, E. R., "Millimeter-wave, terahertz, and mid-infrared transmission through common clothing," *Appl. Phys. Lett.*, vol. 85, pp. 519, 2004.

[5] B. A. Munk, *Frequency Selective Surfaces, Theory and Design*. New York: John Wiley, 2000.

[6] D. W. Poterfield, J.L. Hesler, R. Densing, E.R. Mueller, T.W. Crowe, R.M. Weikle II, "Resonant Metal Mesh Bandpass Filters for the Far-Infrared," *Applied Optics*, vol. 33, pp. 6046, 1994.

[7] M. E. MacDonald, A. Alexanian, R. A. York, Z. Popovic, and E. N. Grossman, "Spectral Transmittance of Lossy Printed Resonant-Grid Terahertz Bandpass Filters," *IEEE Trans. Microwave Theory and Techniques*, vol. 48, pp. 712-718, 2000.

[8] E. N. Grossman, Dietlein, C.R.,Luukanen, A.M., "Terahertz Circular Variable Filters," *4th ESA Workshop on Millimetre-wave Technology and Applications*, pp. 353-358, 2006.
[9] C. Dietlein, Chisum, J.D., Ramirez, M.D., Luukanen, A., Grossman, E.N., Popovic, Z., "Integrated Microbolometer Antenna Characterization from 95-650 GHz," presented at Intl. Microwave Symposium 2007.
[10] T. H. Buettgenbach, "An Improved Solution for Integrated Array Optics in Quasi-optical Mm and Submm Receivers," *IEEE Trans. Microwave Theory and Tech.*. vol. 41, pp. 1750-1761, 1993.
[11] D. F. Filipovic, Gearhart, S.S., Rebiez, G.M., "Double-slot and Log-periodic Antennas on Extended Hemispherical Dielectric Lenses," *IEEE Trans. Microwave Theory and Tech.*. vol. 41, pp. 1738-1749, 1993.
[12] E. R. Brown, McIntosh, K.A., Nichols, K.B., Dennis, C.L., "Photomixing up to 3.8 THz in Low-temperature-grown GaAs," *Appl. Phys. Lett.*, vol. 66, pp. 285-287, 1995.
[13] C. Dietlein, Popovic, Z., and Grossman, E., "Broadband THz Aqueous Blackbody Calibration Source," *Proc. SPIE*, vol. this issue, 2007.
[14] Salmon, N. private communication